doi:10.1016/j.jmb.2011.07.016 J. Mol. Biol. (2011) 413, 297–309

Contents lists available at www.sciencedirect.com

Journal of Molecular Biology

journal homepage: http://ees.elsevier.com.jmb

αB-Crystallin Polydispersity Is a Consequence of Unbiased Quaternary Dynamics

Andrew J. Baldwin[1]*†, Hadi Lioe[2]†, Carol V. Robinson[2], Lewis E. Kay[1]* and Justin L. P. Benesch[2]*

[1]*Departments of Molecular Genetics, Biochemistry and Chemistry, The University of Toronto, 1 Kings College Circle, Toronto, Ontario, Canada M5S 1A8*
[2]*Department of Chemistry, Physical and Theoretical Chemistry Laboratory, University of Oxford, South Parks Road, Oxford, Oxfordshire OX1 3QZ, UK*

Received 25 April 2011; received in revised form 8 July 2011; accepted 11 July 2011
Available online 3 August 2011

Edited by A. G. Palmer III

Keywords:
Polydispersity;
mass spectrometry;
small heat shock proteins (sHSPs);
molecular chaperones;
thermodynamics and kinetics

The inherent heterogeneity of many protein assemblies complicates characterization of their structure and dynamics, as most biophysical techniques require homogeneous preparations of isolated components. For this reason, quantitative studies of the molecular chaperone αB-crystallin, which populates a range of interconverting oligomeric states, have been difficult, and the physicochemical basis for its polydispersity has remained unknown. Here, we perform mass spectrometry experiments to study αB-crystallin and extract detailed information as to its oligomeric distribution and exchange of subunits under a range of conditions. This allows a determination of the thermodynamic and kinetic parameters that govern the polydisperse ensemble and enables the construction of a simple energy profile for oligomerization. We find that the quaternary structure and dynamics of the protein can be explained using a simple model with just two oligomer-independent interactions (i.e., interactions that are energetically identical in all oligomers from 10mers to 40mers) between constituent monomers. As such, the distribution of oligomers is governed purely by the dynamics of individual monomers. This provides a new means for understanding the polydispersity of αB-crystallin and a framework for interrogating other heterogeneous protein assemblies.

Introduction

The vast majority of proteins perform their cellular functions as multimeric assemblies,[1] with interactions ranging from the robust to the fleetingly transient.[2] The preponderance of these protein assemblies is currently thought to exist in one principal oligomeric state, reflective of a defined structure having evolved to perform a particular cellular function.[3] Seemingly contrary to this paradigm, however, some proteins instead populate an ensemble of stoichiometries at equilibrium.

Perhaps the most famous example of such polydispersity is the vertebrate small heat shock protein (sHSP) α-crystallin, which exists in two isoforms (αA and αB) of high sequence similarly.[4] The α-crystallins populate all possible oligomers from between 10 and 40 subunits,[5] a remarkable heterogeneity that has impeded high-resolution structural analysis.[6] Nevertheless, structures of α-crystallin dimers, generated by removal of approximately

*Corresponding authors. E-mail addresses: ajb204@pound.med.utoronto.ca; kay@pound.med.utoronto.ca; justin.benesch@chem.ox.ac.uk.

† A.J.B. and H.L. contributed equally to this work.

Present address: H. Lioe, Bio21 Institute, School of Chemistry, The University of Melbourne, Victoria 3010, Australia.

Abbreviations used: sHSP, small heat shock protein; MS, mass spectrometry; CID, collision-induced dissociation.

0022-2836/$ - see front matter © 2011 Published by Elsevier Ltd.

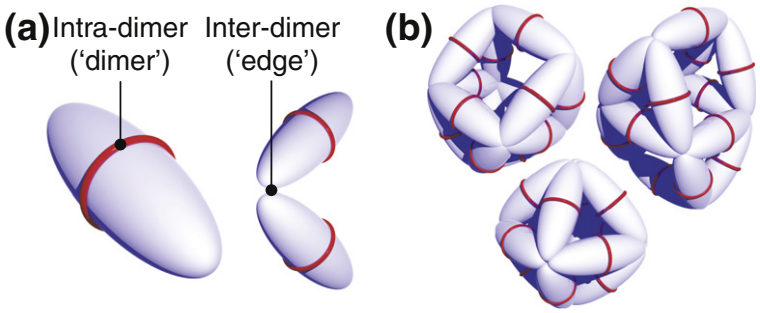

Fig. 1. The oligomeric organization of the sHSPs. (a) The protomeric dimers of αB-crystallin can be represented as ellipsoids, are stabilized by an intra-dimer interface, and assemble into oligomers via inter-dimer interactions. In the model described in this work, these interfaces are termed dimer and edge interactions, respectively, with their strengths described by the corresponding free energies ΔG_d and ΔG_e. (b) These dimers assemble into an ensemble of globular oligomers spanning at least 30 subunits at equilibrium and of unknown structure.

70 N- and 15 C-terminal residues, have been reported.[7–10] These dimers therefore represent the building block of the oligomers[11] and assemble into an ensemble of globular particles.[6,12–14] α-Crystallin structures are therefore stabilized by both intra- and inter-dimer interactions (Fig. 1a).

Despite these structural insights, the origins of the variable stoichiometry of the α-crystallins, vital to the role of this protein in the eye lens,[15,16] are not understood. In addition, the oligomers are known to be very dynamic, with oligomers readily exchanging subunits[17,18] in a process associated with their protective function.[19,20] αB-crystallin is found in many tissues,[15] where, along with other sHSPs, it is central to the maintenance of protein homeostasis.[21] Its molecular chaperone function is to bind and maintain the solubility of unfolded proteins,[22,23] thereby preventing their accumulation into potentially pathogenic aggregates.[24] αB-crystallin malfunction is consequently associated with a range of protein deposition diseases, from cataract formation to Alzheimer's disease.[25] For an appreciation of the mechanism by which αB-crystallin functions as a chaperone, a quantitative understanding of the origins of both the quaternary dynamics and heterogeneity is required.

Nanoelectrospray mass spectrometry (MS) is an emerging structural biology approach, reliably determining the stoichiometries of protein assemblies with unrivalled accuracy.[26–28] Furthermore, through benefiting from very high separation efficiency, it is particularly valuable in the study of polydisperse proteins, allowing the assessment of the oligomers they populate.[29] Though performed in the gas phase, such quantification directly reflects the distribution observed in solution, but with dramatically improved mass resolution.[30–32] This approach has resulted in the quantification of the relative populations of the different oligomers comprising the polydisperse ensemble of the α-crystallins.[5,30,31] Furthermore, the large amount of data obtainable by means of MS in real time makes it well suited to investigating the quaternary dynamics of oligomeric proteins,[33] such as the subunit exchange of the α-crystallins.[31]

Here, we use MS to obtain oligomeric distributions and subunit exchange kinetics of αB-crystallin over a wide range of pH values and temperatures to describe fully the thermodynamic and kinetic basis for its polydispersity. We show that, remarkably, this property can be understood in terms of just two monomer-level interactions, intra- and inter-dimer, which are independent of oligomer size. Furthermore, we demonstrate within the context of this model that formation of α-crystallin oligomer distributions can be explained by the quaternary dynamics associated with single monomers "hopping" between oligomers. As such, the seemingly complex organization of this protein can be rationalized in terms of very simple physical principles, shedding light on how other polydisperse proteins might assemble.

Results

Determining oligomeric distributions and dynamics by means of MS

MS approaches have proven very useful for interrogating the polydisperse αB-crystallin ensemble.[5,30,31,34] A nanoelectrospray mass spectrum of αB-crystallin at pH 7, under conditions optimized for the ionization and transmission of intact protein assemblies, reveals a broad region of signal between 8,000 and 14,000 m/z (Fig. 2a), as is typical for this protein.[5,30,31,34] The extensive overlap of charge states, stemming from the wide range of co-populated stoichiometries, renders the spectrum essentially uninterpretable. To improve the identification of the individual species that comprise the oligomeric ensemble, we employed collision-induced dissociation (CID).[35,36] In this experiment, all ions are accelerated into an argon-filled cell to effect their activation. A spectrum obtained at a high acceleration voltage shows a compact series of peaks at low m/z and a multitude of peaks at 16,000 m/z and above (Fig. 2b). These correspond to monomers and complementary "stripped" oligomers, that is,

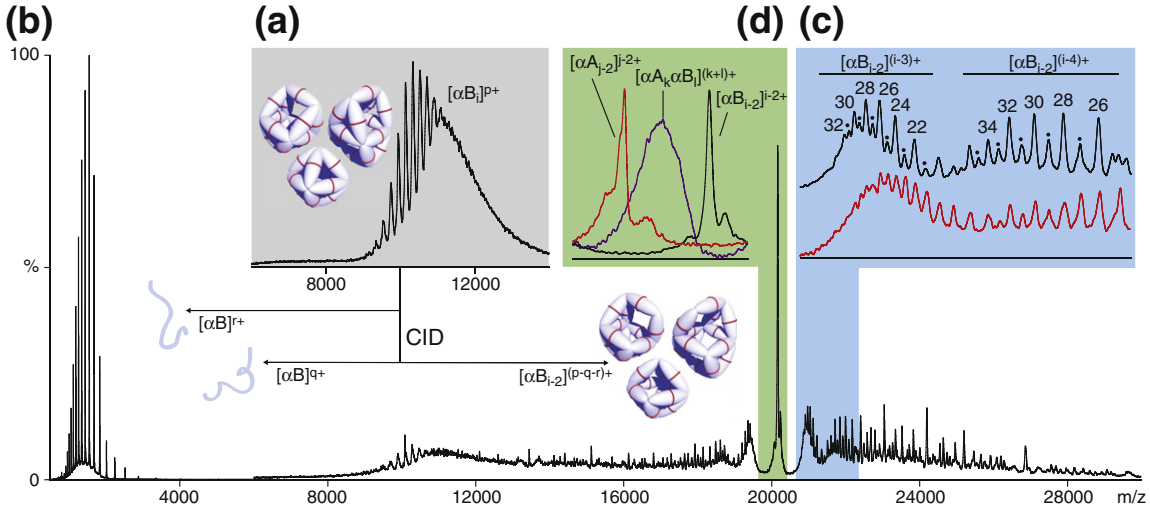

Fig. 2. Nanoelectrospray MS of αB-crystallin. (a) The mass spectrum of αB-crystallin is typical of what is observed for a heterogeneous protein ensemble, with the peaks corresponding not to individual charge states but, rather, resulting from the accumulation of a number of charge states from many different species $[\alpha B_i]^{p+}$. (b) A mass spectrum as in (a) but obtained under activating conditions in which all ions are submitted to energetic collisions with argon atoms. Peaks are observed at both low and high m/z corresponding to highly charged monomers, $[\alpha B]^{r+}$ and $[\alpha B]^{q+}$, and complementary stripped oligomers, respectively. This is in agreement with the general mechanism of gas-phase protein complex dissociation. The area between ~18,000 and 25,000 m/z corresponds to αB-crystallin oligomers stripped of two monomers, $[\alpha B_{i-2}]^{(p-q-r)+}$ and has resolution sufficient to allow the identification and relative quantification of the individual species (c). Note that even values of i are shown above selected peaks; the peaks corresponding to oligomers with an odd number of subunits are located between these (black dots). From this, the complete oligomeric distribution of αB-crystallin can be derived. Spectra are shown for pH 7 (black) and pH 5 (red), with the odd oligomers being significantly more prevalent at pH 5. (d) The peak at ~21,500 m/z (black) corresponds to all αB-crystallin doubly stripped oligomers carrying as many charges as subunits $[\alpha B_{i-2}]^{(i-2)+}$. The equivalent peak for αA-crystallin appears at ~19,800 (red), whereas a fully equilibrated mixture of the two isoforms gives a broader peak between the two, representing the distribution of hetero-oligomers.[31]

αB-crystallin oligomers having lost one or more monomers, respectively.[5] This sequential removal of highly charged monomers leads to an effective charge reduction of the parent ions, such that individual oligomeric stoichiometries can be identified unambiguously (Fig. 2c).[35] In this way, a range of oligomeric states of αB-crystallin is observed at pH 7 (Fig. 2c, black), centered on a 28mer. Moreover, from the intensities of the peaks, the relative abundance of each species can be extracted, providing a basis for the quantification of the thermodynamics of the αB-crystallin ensemble, as described below. It is notable that, at pH 7, oligomers with an even number of subunits are considerably more abundant than those with an odd number.[30] An equivalent spectrum obtained at pH 5 shows a remarkable difference (Fig. 2c, red), namely, this preference for even oligomers is dramatically reduced, revealing that the strength of the intra-dimer interface is pH sensitive, as described in detail below.

The peak at ~20,150 m/z (Fig. 2d, black) corresponds to αB-crystallin oligomers stripped of two monomers, each carrying as many charges as subunits, and therefore, it contains a contribution from all oligomers within the ensemble.[5] The equivalent peak, obtained from identical experiments, for αA-crystallin appears at ~19,800 m/z (Fig. 2d, red), due to the slightly lower molecular mass at the sequence level. Incubation of the two proteins results in subunit exchange, manifested in the mass spectrum by the coalescence of the peaks corresponding to the homo-oligomers into a broad peak centered on their midpoint (purple).[31] By obtaining of spectra at different time points, the course of subunit exchange can be monitored, discussed in detail below, allowing a detailed quantitative analysis of the quaternary dynamics of this protein.

A Poisson distribution describes the heterogeneity of αB-crystallin at low pH

MS measurements reveal broad oligomeric distributions that are highly pH sensitive (Fig. 2c; Fig. 3a, red). At low pH, the distribution is smooth, while at higher pH, it becomes more uneven, with a preference for oligomers comprising an even number of subunits. By contrast, the distribution does not vary appreciably with temperature.[37] The fact that both odd and even oligomers are observed in all distribution profiles means that the exchange must,

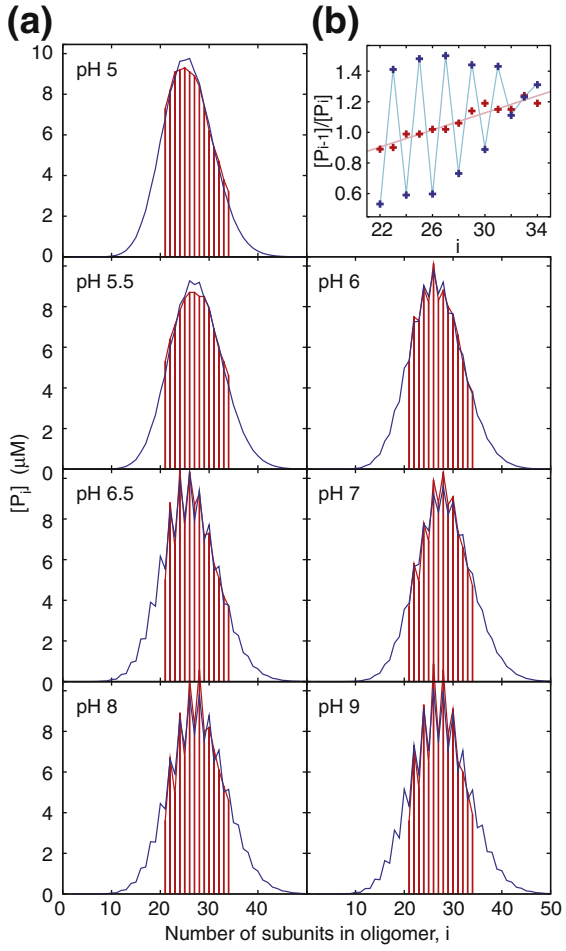

Fig. 3. Oligomeric distributions of αB-crystallin as a function of pH. (a) Distributions were obtained for pH 5–9 at 37 °C and are normalized to the total protein concentration. Experimental data are shown in red, and the calculated distributions are in blue, where $[P_i]$ is the concentration of an oligomer consisting of i monomers. Calculated distributions (blue) were obtained using Eqs. (5)–(7.2) to produce ΔG_e and ΔG_{e+d} values shown in Fig. 4 (see Methods). (b) The ratio $[P_{i-1}]/[P_i]$ as a function of oligomer size at pH 5 (red) and pH 9 (blue). The ratio depends linearly on i at pH 5 (red line), from which it follows that the size distribution at this pH obeys Poisson statistics. The Pearson R^2 correlation coefficient for the ratio at pH 5 and subunit size is 0.99.

at least in part, be mediated by the movement of monomers. In fact, we show immediately below that the equilibrium distributions observed can be well described as arising from the exchange of individual subunits between parent oligomers, an assumption that is further validated through NMR studies.[38]

A simple exchange scheme can be constructed that can explain the experimental results by considering the successive accumulation of monomers to form oligomers (monomer exchange),[39] $\left\{ P_1+P_1 \underset{k_2^-}{\overset{k_2^+}{\rightleftharpoons}} P_2, P_1+P_2 \underset{k_3^-}{\overset{k_3^+}{\rightleftharpoons}} P_3, \ldots P_1+P_{i-1} \underset{k_i^-}{\overset{k_i^+}{\rightleftharpoons}} P_i \right\}$, where P_1 is a free subunit in solution, P_i is an oligomer of i subunits, and $k_j^-/k_j^+\{j \in (2,\ldots,i)\}$ are dissociation/association rate constants. An association equilibrium constant, $K_j^A = \frac{[P_j]}{[P_{j-1}][P_1]}$, can be ascribed to each binding step involving the formation of oligomer j above. Within this scheme, the general rate equations for the time dependence of the concentration of each oligomer P_i $(i \neq 1)$ and free monomer P_1 are:

$$\frac{d[P_i]}{dt} = -k_i^-[P_i] + k_i^+[P_{i-1}][P_1] - k_{i+1}^+[P_i][P_1] + k_{i+1}^-[P_{i+1}] \quad (1)$$

$$\frac{d[P_1]}{dt} = \sum_2^n k_i^-[P_i] + k_2^-[P_2] - \sum_2^n k_i^+[P_1][P_{i-1}] - k_2^+[P_1]^2 \quad (2)$$

Both equations are satisfied at equilibrium if $[P_i] = \frac{k_i^+}{k_i^-}[P_1][P_{i-1}]$, from which it follows that $K_i^A = \frac{k_i^+}{k_i^-}$. Therefore, the concentration of an oligomer at equilibrium can be calculated if the total protein concentration and the rates k_i^+ and k_i^- are known for all sizes of interest using the relation $[P_i] = [P_1]^i \prod_{j=2}^{i} \left(\frac{k_j^+}{k_j^-}\right)$, $i>1$. In the case of αB-crystallin at pH 5, the ratio $\frac{[P_{i-1}]}{[P_i]}$ was found experimentally to vary linearly with i such that $\frac{[P_{i-1}]}{[P_i]} = \frac{i}{M_A}$, where M_A is a constant (Fig. 3b, red points). From the definition above of the association equilibrium constant, it follows that $\frac{[P_{i-1}]}{[P_i]} = \frac{k_i^-}{k_i^+[P_i]}$, so that at pH 5

$$\frac{i}{M_A} = \frac{k_i^-}{k_i^+[P_1]} \quad (3)$$

and the ratio of the dissociation and association rates varies linearly with increasing oligomer size. It can be shown that, in this case, the oligomer distribution must follow a discrete Poisson distribution, a special case of a Gaussian distribution, where the mean and the variance are equal,[31] $[P_i] \propto \frac{1}{i!}(M_A)^i$. A consequence of the Poisson distribution is that the constant M_A is equal to both the mean oligomer size and the variance of the distribution. In other words, the heterogeneity and the average size of αB-crystallin are intrinsically linked.

The simplest kinetic model is obtained by setting the dissociation rate of a given oligomer to be proportional to the number of component subunits such that $k_i^- = ik^-$, with the association rate independent of oligomer size, $k_i^+ = k^+$. Such a situation arises when (i) the environments of all monomers are essentially the same in all oligomers, as supported

by the NMR spectra of αB-crystallin showing a single cross peak for each probe;[11,38] (ii) each monomer is equally likely to dissociate from its parent oligomer at any time; and (iii) there is effectively a single binding (association) site on the oligomer, independent of its size. Physically, the condition $k_i^+ = k^+$ can arise if the rate-limiting step of association reflects the initial binding of a free monomer to the oligomer, with subsequent internal rearrangements occurring significantly more rapidly. From Eq. (3) and the assumption $k_i^- = ik^-$, $k_i^+ = k^+$, it follows directly that $M_A = \frac{k^+[P_1]}{k^-}$. Thus, within the framework of our model, monomers exchange between oligomers at low pH with microscopic association (k^+) and dissociation rate constants (k^-) that are independent of the size of the exchanging partners. This model completely reproduces the low-pH MS data [Fig. 3a and b, red].

In a companion paper,[38] we show that the proposed kinetic model can also explain relaxation dispersion NMR data, providing additional support but not proof of our kinetic scheme. We have explored a range of additional monomer exchange models including helical and linear polymerization schemes,[40,41] which cannot explain our experimental data (Fig. S1). Further, more elaborate schemes involving the exchange of fragments larger than single monomers have also been considered. With similar simplifying assumptions such as $k_i^- = k^-$, $k_i^+ = k^+$ and $k_i^- = ik^-$, $k_i^+ = k^+$, such models do not yield equilibrium distributions that resemble the experimental data (Fig. S1). Finally, it is worth noting that our model can be contrasted with the case of the sequential dissociation/association of a ligand from a macromolecule containing n equivalent binding sites, $PL_{i-1} + L \underset{k_i^-}{\overset{k_i^+}{\rightleftharpoons}} PL_i$, where the oligomeric association and dissociation rates are given by $k_i^- = ik^-$ and $k_i^+ = (n\text{-}i\text{+}1)k^+$, respectively.[42]

The dimer interface is strengthened at higher pH

As the pH is increased, the observed size distributions become uneven, with a preference for oligomers composed of an even number of subunits (Fig. 3a), and thus no longer follow Poisson statistics (Fig. 3b, blue). The model described above must therefore be expanded slightly to take this into account.

A slight preference for αB-crystallin to populate "even-numbered" stoichiometries indicates the presence of some dimeric substructure within the oligomers.[11,30] This is consistent with atomic-resolution structural data that have revealed that monomers of αB-crystallin assemble into dimers by sharing an interface between extended β-strands[7,9] and that this interface is very labile (Fig. 1a).[8,43] In order to assemble into oligomers, these intra-dimer interactions must be complemented by inter-dimer interactions (Fig. 1a). In what follows, we refer to these two classes of contacts as "dimer" (intra-dimer) and "edge" (inter-dimer) interactions, respectively. It is important to stress that we make no assumptions as to the structural origins of these edge interactions and, in principle, they could involve several contacts.

In our model, we assume that all monomers within an oligomer make the maximum allowed number of such interactions in order to minimize each monomer free energy. Thus, in the case of an oligomer consisting of an even number of monomers, all dimer and edge interactions are satisfied, while for an odd-numbered oligomer, a single monomer lacks dimer contacts (referred to as an unpaired monomer). When dimer contacts are much less significant than edge interactions, it is expected that the kinetic rates describing the addition/subtraction of a monomer would be essentially the same, irrespective of whether the binding event involves an even- or odd-numbered oligomer. This assumes that the nature of the edge contacts is unchanged in the odd/even cases. Such a situation emerges at low pH, where edge interactions dominate and where the dissociation kinetics are well described by a single microscopic rate, k^-. As the contribution to the stability of the oligomer from dimer contacts increases, however, it is expected that microscopic dissociation rates would not be the same for unpaired and paired monomers (Fig. 4a). This is because an unpaired monomer would be attached more weakly than all of the other monomers so that its dissociating rate, k_e^-, would be greater than the corresponding value for removal of a "paired" monomer from the oligomer k_{e+d}^-. Thus, Eq. (1) is modified according to

$$\begin{aligned} P_1 + P_{i-1} \underset{ik_{e+d}^-}{\overset{k^+}{\rightleftharpoons}} P_i, \quad \frac{d[P_i]}{dt} = & -ik_{e+d}^-[P_i] + k^+[P_{i-1}][P_1] \\ & - k^+[P_i][P_1] + \left(ik_{e+d}^- + k_e^-\right) \\ & \times [P_{i+1}], \quad i = \text{even} \end{aligned} \tag{4.1}$$

and

$$\begin{aligned} P_1 + P_{i-1} \underset{(i-1)k_{e+d}^- + k_e^-}{\overset{k^+}{\rightleftharpoons}} P_i, \quad & \frac{d[P_i]}{dt} \\ = & -\left\{(i-1)k_{e+d}^- + k_e^-\right\}[P_i] + k^+[P_{i-1}][P_1] \\ & - k^+[P_i][P_1] + (i+1)k_{e+d}^-[P_{i+1}], \quad i = \text{odd} \end{aligned} \tag{4.2}$$

where explicit use has been made of our assumption $k_i^- = ik^-$, $k_i^+ = k^+$ (see above). Note that the factor $ik_{e+d}^- + k_e^-$ preceding $[P_{i+1}]$ in Eq (4.1) derives from the fact that, in a particle consisting of $i+1$ monomers (i is even), there are i paired monomers and one that is unpaired. Thus, for each of the i paired interactions, dissociation must proceed through breaking edge and dimer interactions (k_{e+d}^-), while for the unpaired contact, only the edge interactions

must be released (k_e^-). This situation is illustrated schematically for the case of a 23mer in Fig. 4a. It follows directly from Eqs. (4.1) and (4.2) that the concentration of each oligomer is given by

$$[P_i]_{even} = \frac{k^+[P_1]}{ik_{e+d}^-}[P_{i-1}] = \frac{M_A}{i}[P_{i-1}] \quad (5)$$

$$[P_i]_{odd} = \frac{k^+[P_1]}{(i-1)k_{e+d}^- + k_e^-}[P_{i-1}] = \frac{M_A}{i-1+n}[P_{i-1}] \quad (6)$$

where $k_e^- = nk_{e+d}^-$, n is a multiplier greater than or equal to 1, and as before $M_A = \frac{k^+[P_1]}{k_{e+d}^-}$. In the limit where $n=1$, $k_e^- = k_{e+d}^- = k^-$ and a Poisson distribution is obtained, as discussed above. The relative free-energy difference between a given oligomer of size i and the corresponding oligomer of size $i-1$, created through the loss of a monomer from a single, specific site as depicted in Fig. 4b, is given by

$$\Delta G_{e+d} = G_{i,e+d} - G_{i-1,e+d} = -RT\ln\frac{[P_1]k^+}{k_{e+d}^-} = -RT\ln(M_A) \quad (7.1)$$

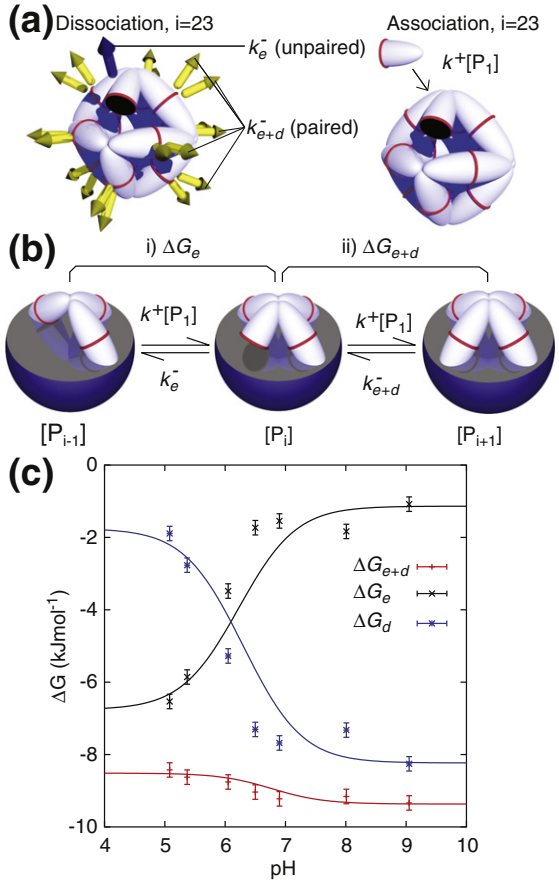

$$\Delta G_e = G_{i,e} - G_{i-1,e} = -RT\ln\frac{[P_1]k^+}{k_e^-} = -RT\ln\left(\frac{M_A}{n}\right) \quad (7.2)$$

depending on whether i is even (ΔG_{e+d}, added monomer is paired) or odd (ΔG_e, added monomer is unpaired). It follows that the stability of the dimer interface is given by

$$\Delta G_d = \Delta G_{e+d} - \Delta G_e = -RT\ln n \quad (7.3)$$

Note that all three quantities ΔG_{e+d}, ΔG_e, and ΔG_d are independent of i, the number of subunits within the oligomer. This model therefore allows fitting of the experimental size distributions obtained from MS at all pH values and temperatures with ΔG_e and ΔG_d as free parameters. The fits reproduce the experimental data extremely well (Fig. 3a and Fig. S2), demonstrating that our model

Fig. 4. Thermodynamics of the oligomeric distribution of aB-crystallin. (a) Schematic showing the association and dissociation pathways for a 23mer structure (based on an octahedron, with dimers placed on each of the edges). As in Fig. 1, each dimer is represented by a white ellipsoid, with the dimer interface denoted by a red collar, while the single monomer is indicated by half an ellipsoid. Dissociation may take place through the loss of a paired monomer with rate k_{e+d}^- (yellow arrow) or an unpaired monomer with rate k_e^- (blue arrow). In the case of the 23mer, the rate of loss through dissociation is $22k_{e+d}^- + k_e^-$ (contributions from 22 paired monomers and 1 unpaired monomer). Each of the 22 paired monomers is equally likely to dissociate in any given time period. Association of a monomer with a 23mer to form a 24mer is independent of the number of oligomers and occurs with a rate of $k^+[P_1][P_{23}]$. In the limit where the dimer interface is relatively strong ($k_e^- > k_{e+d}^-$), unpaired monomers are easily lost and even oligomers are favored, as observed at high pH. In the limit where the dimer interface is relatively weak ($k_e^- \approx k_{e+d}^-$), the equilibrium profile is well approximated by a smooth Poisson distribution, as observed at low pH. (b) Schematic showing the physical origin of the two free-energy parameters required to fit the MS distribution data. The sphere represents an oligomer, with interactions between groups of dimers within the oligomer indicated. (i) Free-energy change on adding a single "unpaired" monomer, ΔG_e, to an even-numbered oligomer where only the edge interactions are formed, along with the microscopic rate constants describing rates of association with and dissociation from a specific site. The dissociation rate of the unpaired monomer is faster than that of a paired monomer ($k_e^- > k_{e+d}^-$). (ii) Free-energy change on adding a single "paired" monomer to an odd oligomer, $\Delta G_{e+d} = \Delta G_e + \Delta G_d$. Note that the dissociation rate from each site is k_{e+d}^- so that the net rate of monomer release for an oligomer with i paired monomers is ik_{e+d}^-. Values of ΔG_{e+d}, ΔG_e, k_e^- and k_{e+d}^- are independent of oligomer size. (c) Variation in ΔG_{e+d}, ΔG_d, and ΔG_e as a function of pH, 37 °C, demonstrates that the dimeric interface is weakened at low pH, while the inter-dimer edge interaction is strengthened.

provides a good description of the oligomerization of αB-crystallin (Fig. 3a, blue) and allowing an estimation of the strength of the inter- and intra-dimer interactions. The variation of ΔG with pH establishes that, at low pH, the edge interactions dominate those at the dimer interface (Fig. 4c). By contrast, at high pH, the importance of these contributions is reversed, leading to a preponderance of even-numbered oligomers. Notably, the free-energy ΔG_{e+d}, which dictates the average oligomer size, varies little with pH. It is worth noting that, even for pH values ≥ 6, where the distribution clearly favors even-numbered oligomers, the profiles are well explained by a model that assumes monomer exchange exclusively. In the companion paper to this article, it is shown, further, that the timescale for dimer exchange is inconsistent with the rate of subunit exchange measured by MS[38] (see below).

It is interesting to note that oligomer size distributions are observed to be independent of total protein concentration over 3 orders of magnitude, implying that $[P_1]$ is invariant (buffered) over this range.[4] Such behavior is anticipated by our model, and it is possible to show that $\frac{d[P_1]}{d[P_{Total}]} \approx 0$ in the experimentally accessible concentration regime. This is similar to what is found at equilibrium in linear and helical polymerization assembly models.[41,44]

The quaternary dynamics vary in a marked fashion with both pH and temperature

The thermodynamic parameters obtained by fitting equilibrium population distributions do not provide unique rates of oligomer assembly and dissociation. To obtain complementary kinetic information, we have performed time-resolved MS experiments to monitor the exchange of subunits between oligomers of αB- and αA-crystallins (Fig. 5a). The m/z range monitored represents all oligomeric species within the ensemble, with αA- and αB-crystallin homo-oligomers giving rise to peaks at ~19,800 and ~21,500 m/z, respectively (Fig. 2d). Initially, these two distinct populations are observed, but upon incubation, they coalesce to produce an equilibrium distribution of hetero-oligomers containing both isoforms (Fig. 5a).[31] At 37 °C, pH 5, this process is complete within 1 min, whereas, at the same temperature but at pH 9, full exchange is only reached after approximately 5 h, consistent with previous studies.[18] In order to

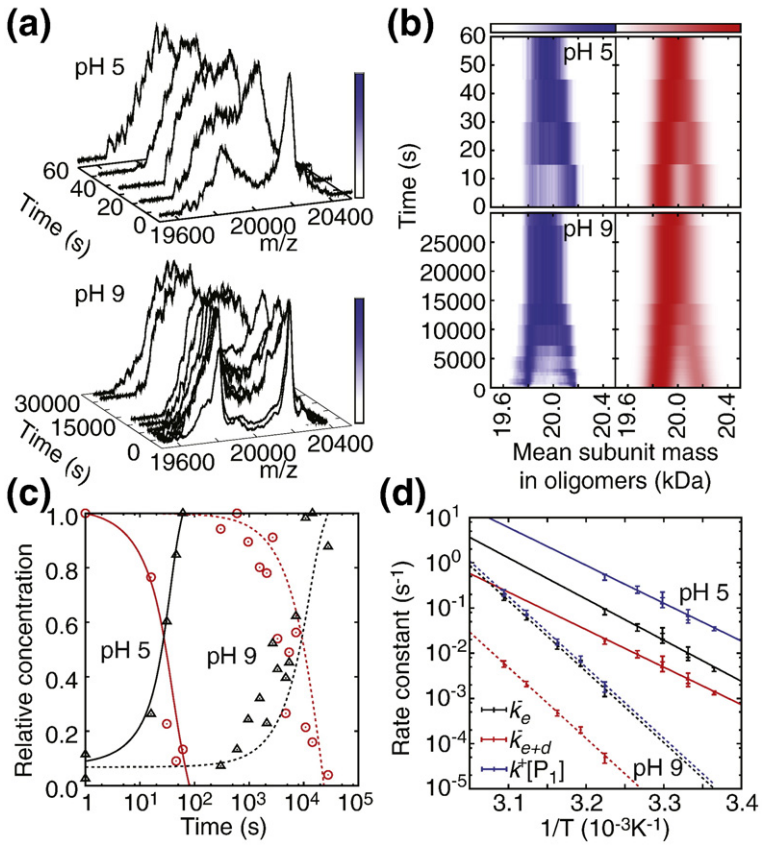

Fig. 5. Kinetics of α-crystallin subunit exchange. (a) Subunit exchange time course at 37 °C, pH 5 (upper) and pH 9 (lower), monitored by using MS, c.f. Fig. 2d, shows the coalescence of the two homo-oligomer peaks into a single peak representing the distribution of hetero-oligomers. This m/z range corresponds to doubly stripped oligomers carrying the same number of charges as subunits $[\alpha B_{i-2}]^{(i-2)+}$, meaning that, in this range, m/z is equivalent to the average mass of the subunits comprising the oligomer in question. (b) Alternative "top-down" view of the data (left), compared to the simulated time courses that best fit the experiment (right). (c) One-dimensional "slices" of (b), demonstrating the loss of homo-oligomers (red) and the gain of hetero-oligomers (black) along with the simulation that best matches the experiment at pH 5 (continuous lines) and pH 9 (dotted lines). The high precision of the experimentally determined rate constants (Fig. S2b) arises from the accuracy with which the point of coalescence can be determined when analyzing two-dimensional data of the type shown in (b). (d) Variation in k_e^-, k_{e+d}^-, and $k^+[P_1]$ with temperature at pH 5 (continuous lines) and pH 9 (dotted lines). Only these three parameters are necessary to explain the kinetics and thermodynamics of oligomer formation and size distribution.

quantify the time dependence of this mixing process in terms of the pseudo-first-order association rate $k^+[P_1]$ and dissociation rate constants for paired (k_{e+d}^-) and unpaired (k_e^-) monomers, we performed simulations to reproduce the experimental data (Fig. 5b and c). Best-fit values of $k^+[P_1]$, k_{e+d}^-, and k_e^- were therefore obtained as a function of temperature, in the range 24–50 °C, at both pH 5 and pH 9. Under the conditions examined, rate constants were determined to a precision of ±5% on average (Fig. S2) and vary by 4 orders of magnitude, with rates increasing at higher temperature and lower pH (Fig. 5d). The data were found to show Arrhenius behavior, allowing activation parameters ΔH^* and ΔS^* to be calculated (Table S1), following transition state theory (see Methods).

Under all conditions, the concentration of free monomer (and oligomer concentrations for sizes less than approximately 10 monomers, Fig. 3a) was too small to detect, and hence, the first-order rate constant k^+ could not be obtained (only the pseudo-first-order rate, $k^+[P_1]$). Nonetheless, limits can be placed on the free monomer concentration and, hence, on the association rate k^+. First, an estimate for the upper limit of $[P_1]$ can be made by considering the noise level in measured MS data sets. The lower limit of monomer detection is ca 10 nM (upper bound for $[P_1]$), 3 orders of magnitude lower than the concentration of the 24mer (40 μM total sample concentration). With such an estimate, the microscopic association rate constant k^+ varies between $\approx 10^5$ M^{-1} s^{-1} (pH 5, 30 °C; pH 9, 40 °C) and $\approx 10^7$ M^{-1} s^{-1} (pH 5, 40 °C; pH 9, 50 °C). Note that association rates on the order of 10^7 M^{-1} s^{-1} are close to the diffusion limit,[45] indicating that association is rapid. A lower limit for $[P_1]$ can be obtained by assuming that the association rate is at the diffusion limit ($\approx 10^7$ M^{-1} s^{-1}). Under this assumption, $[P_1]$ varies between ≈0.1 nM (pH 5, 30 °C; pH 9, 40 °C) and ≈10 nM (pH 5, 40 °C; pH 9, 50 °C). Thus, an approximate concentration range for free monomer in solution is $0.1\ \text{nM} \le [P_1] \le 10\ \text{nM}$ under the experimental conditions employed.

Discussion

The distribution and subunit exchange experiments we have described here have provided a detailed picture of αB-crystallin quaternary dynamics and organization in terms of the thermodynamic and kinetic properties that relate to the association and dissociation of individual monomers. We have shown that the complex polydisperse ensemble and the underlying quaternary dynamics can be explained purely by the movement of monomers (see also our companion paper[38]) and in terms of three oligomer-size-independent parameters, $k^+[P_1]$, k_e^-, and k_{e+d}^-. The stability increase accompanying binding of monomer to a growing oligomer favors particles of increasing size. This tendency, in turn, is balanced by a net dissociation rate that grows linearly with oligomer stoichiometry, leading naturally to a maximum in the distribution profile, as observed in the MS data. The kinetic parameters extracted here depend strongly on pH and temperature, with the unimolecular process of subunit loss rate limiting. As such, we have presented a means for understanding the underlying physical basis by which αB-crystallin populates a polydisperse ensemble at equilibrium.

Our data show a clear pH dependence to the strength of both the intra- and the inter-dimer interactions. At low pH, the dimer interface is weakened considerably, in agreement with studies performed on a stabilized α-crystallin dimer,[43] and can be understood in terms of the network of charged interactions at the interface.[46] The pH variation in ΔG_d is compensated by that of ΔG_e, with the edge interface becoming stronger with decreasing pH (Fig. 4c). This remarkable self-compensatory behavior ensures that, in essence, the sum of the two free energies, a quantity that is directly related to both the average oligomer size and polydispersity [Eq. (7.1)], is conserved. It therefore appears that αB-crystallin has evolved to maintain a constant average oligomeric size that is resistant to variations over an exceedingly broad range of pH (5–9) and temperature (20–50 °C). This can be understood in terms of the role of α-crystallin in maintaining eye lens transparency while avoiding crystallization.[16] Entropy and enthalpy compensation is a well-known phenomenon in biophysics[47] and underlies the workings of many allosteric protein machineries.[48] Recent studies of αB-crystallin dimers provide an interesting clue as to the structural origins of this compensation, namely, changes in the curvature of and loop orientations within the dimeric building blocks as a function of either pH or mutation of interface residues.[8,11] Such changes in conformation of the dimer would be expected to relax or strain the inter-dimer interactions.

In the case of a homogeneous, monodisperse oligomeric assembly, specific interactions lead to one oligomeric form becoming overwhelmingly dominant within the ensemble,[49] as is the case for the crystallized sHSP oligomers.[50,51] However, for αB-crystallin, the specificity of these interactions is relaxed, as the polydispersity stems from relatively promiscuous quaternary dynamics that allow a monomer to recombine with any sized oligomer. The question arises as to the functional role of this polydispersity. It has been postulated that, through hampering of crystallization despite the extremely high protein concentrations, polydispersity is important for maintaining transparency of the eye lens.[16] However, it is important to consider that αB-crystallin is still polydisperse at the lower

concentrations in which it is found in other tissues,[4] as indeed are other human sHSPs such as HSP27.[52] Furthermore, we have recently shown that a plant sHSP undergoes a monodisperse-to-polydisperse transition upon activation, leading to formation of a broad range of stoichiometries between the sHSP and the client protein.[53] Taken together, this suggests that the polydispersity and quaternary dynamics play an important role in cellular sHSP chaperone function.

Our results also have implications for the molecular mechanism by which αB-crystallin prevents aggregation of target proteins. It has been postulated that activity results from the encounter between sub-oligomeric forms of the sHSP with unfolding protein, with oligomer dissociation amounting to an activation of the chaperone.[19,20,54] Interestingly, however, αB-crystallin is able to curtail the precipitation of insulin at 25 °C, pH 7, on a timescale of approximately 1 h.[55] Under these conditions, the rate of monomer dissociation is 5.3×10^{-6} s^{-1}, equivalent to a subunit exchange timescale of over 50 h . At least in this case, it is likely that the primary event for chaperone activity is not the encounter between target protein and free αB-crystallin monomer but, rather, with an oligomeric form of the chaperone. This is consistent with a cross-linking study on α-crystallin,[56] previous work on the dynamics of αA-crystallin,[18] and our investigation of a truncated form of the same protein that displayed a reduced subunit exchange rate but no decrease in suppression of aggregation *in vitro*.[31] Through comparative kinetic measurements, the quantitative approach we have developed here provides a means for addressing this aspect of sHSP chaperone action in future studies.

An alternative activation mechanism, based upon changes in oligomerization from single stoichiometry to polydisperse ensemble, has been observed for HSP18.1 from pea.[53] Such a scenario may be relevant here. As we observe no change in the oligomeric distribution of αB-crystallin with temperature, it would appear that the ensemble of oligomeric states that have been characterized in the present study represents the active chaperone state of αB-crystallin. The dramatic differences in interface strengths and kinetics we observe as a function of pH might act to regulate the chaperone activity of this protein. Indeed, differences in chaperone activity have been noted *in vitro* as a function of pH.[57–59] This is pertinent to two tissues where αB-crystallin is known to perform a protective chaperone role: the eye lens and cardiac muscle. In the former, there is a pH gradient across the lens, with the center of the lens, populated by the oldest, most posttranslationally modified, and hence aggregation-prone lens proteins, being considerably more acidic than the periphery.[60,61] Similarly, during an ischemic episode, the pH of the cardiac cell cytosol is known to drop.[62] Both of these circumstances provide clear examples where pH regulation of αB-crystallin activity would act to protect the cell from the deleterious consequences of protein aggregation and deposition.

Previous studies have shown that mimicking phosphorylation results in a loss of a preference for αB-crystallin oligomers with an even number of subunits.[30,63] Interpreted in the context of the model described here, this observation implies a weakening of the dimeric interface, similar to what we have shown here with wild-type protein upon acidification. Applying the quantitative approach described in the present work has enabled us to extract the thermodynamic consequences of this phosphomimicking (Fig. S3). Consistent with our previous study,[30] we find that, at 37 °C and pH 7, the mutation S19D gives a distribution identical to that of the wild-type protein and the double mutant S19/45D results in a dramatic increase in ΔG_d (from −7.7 to −4.3 kJ/mol) with a compensatory decrease in ΔG_e (from −1.5 to −3.9 kJ/mol). The triple mutant S19/45/59D results in a further destabilisation of the dimer interface, with a change in ΔG_d to −0.79 kJ/mol and a compensatory effect on ΔG_e (−7.43 kJ/mol). Strikingly, the double mutant is therefore approximately equivalent to making the protein behave at pH 7 as the wild-type does at pH 6, and the triple mutant makes the protein behave at pH 7 as the wild type does at pH 5. While the specifics of how these variations in interface strengths control chaperone activity *in vivo* remain to be elucidated, this provides evidence for different regulatory mechanisms for αB-crystallin operating via a common pathway.

This work has shown the inherent link between the movement of single αB-crystallin subunits between different oligomeric forms and the resultant large particle size distributions. The ability to adopt a range of oligomeric forms and to do so on the timescale of minutes likely underpins the promiscuous and versatile interactions that this protein can make. Furthermore, our demonstration that the complex oligomerization behavior of αB-crystallin can be explained in terms of two monomer-level interactions provides a template for similar understanding of other polydisperse proteins.

Methods

Obtaining oligomeric distributions

αB- and αA-crystallins were expressed in *Escherichia coli* and purified using standard approaches.[64] To investigate the distribution of oligomeric stoichiometries populated by αB-crystallin, we employed nanoelectrospray MS under solution and instrument conditions optimized for the preservation of non-covalent interactions.[65] No

monomers or oligomers containing fewer than 10 subunits are observed in the spectra, demonstrating that there is no dissociation of the oligomers during transfer into the gas phase. Solutions of αB-crystallin were prepared at a monomeric concentration of 50 μM in 200 mM ammonium acetate, at the specified pH. Samples were analyzed on a Q-ToF 2 mass spectrometer (Waters UK Ltd.), modified for the study of large protein assemblies,[66] using previously described instrument settings.[5]

CID was performed by accelerating all species, without selection in the quadrupole analyzer, into a collision cell pressurized with 35 μbar of argon.[5] The resulting doubly stripped oligomers, those derived from the removal of two successive highly charged monomers, are spread over a wide m/z range and can thereby be identified unambiguously and, due to charge conservation, can be related directly to their parent oligomer.[5,35] Moreover, as no other dissociation pathways are operative, during either ionization or activation, the relative abundances can be quantified from the intensity of the peaks corresponding to the all charge states observed for each of the doubly stripped oligomers, as described previously[5] and as illustrated in Fig. 2. It is important to note that the reproducibility of these experiments is very high, with the relative abundances of oligomers varying by less than ±5% between replicate experiments,[53] a value comparable to the uncertainties in the quantities back calculated using the model (Fig. S2).

Optimum values of M_A and n and hence values of ΔG_{e+d}, ΔG_e, and ΔG_d [see Eqs. (7.1)–(7.3) in the text] were obtained as follows. The total concentration of monomers in the system is given by $[P]_{Total} = \sum_{i=1}^{N} i[P_i]$, with the concentration of a given oligomer expressed as

$$[P_i] = [P_1]^i \prod_{j=2}^{i} \left(\frac{k_j^+}{k_j^-}\right), i > 1 \tag{8}$$

Rearranging Eq. (8) so that

$$[P_i] = [P_1] \prod_{j=2}^{i} \frac{[P_1]k_j^+}{k_j^-}, i > 1 \tag{9}$$

it follows that

$$[P]_{Total} = [P_1] + [P_1] \sum_{i=2}^{N} i \prod_{j=2}^{i} \frac{[P_1]k_j^+}{k_j^-} \tag{10}$$

where from Eqs. (5) and (6) of the text

$$\begin{aligned} \frac{k_j^+[P_1]}{k_j^-} &= \frac{k^+[P_1]}{jk_{e+d}^-} = \frac{M_A}{j}, \text{ even } j \\ \frac{k_j^+[P_1]}{k_j^-} &= \frac{k^+[P_1]}{(j-1)k_{e+d}^- + k_e^-} = \frac{M_A}{(j-1+n)}, \text{ odd } j \end{aligned} \tag{11}$$

The total monomer concentration was determined by measuring the absorbance of the solution at 280 nm using an extinction coefficient of 13,980 M^{-1} cm^{-1}. Our limit of detection is determined from the signal-to-noise ratio in the spectrum, taking into account the m/z dependence of multichannel plate sensitivity.[67] For a given choice of M_A and n, Eq. (10) is solved for $[P_1]$ from which $[P_i]$ is obtained via Eq. (9). Consequently, each oligomer concentration depends only on $[P]_{Total}$, M_A, and n. Values of M_A and n are, in turn, obtained via minimization of the χ^2 target function $\sum_{i=1}^{N} \left([P_i]_{exp} - [P_i]_{calc}\right)^2$.

Quantifying the kinetics of subunit exchange

We probed the quaternary dynamics of αB-crystallin by mixing it with its lighter isoform, αA-crystallin. The rate of subunit exchange is known to be isoform independent[68] and is very low at reduced temperature.[18] After incubation of the reaction mixture for various times, quenching of a given aliquot was achieved by chilling on ice, allowing off-line analysis by means of nanoelectrospray MS as described above. Mass spectra were obtained under CID conditions, with the doubly stripped oligomer region examined for quantitative analysis. By monitoring the peaks corresponding to those doubly stripped oligomers carrying as many charges as subunits, we obtained the time dependence of the disappearance of homo-oligomers and the concomitant appearance of hetero-oligomers, as described previously.[31,32]

The time courses are then analyzed in detail by fitting the experimental data to the general rate equations describing the time evolution of the concentration of an oligomer containing i and j monomers of type I (αB) and type II (αA) during an equilibration period,

$$\begin{aligned} \frac{d[P_{i,j}]}{dt} = & -ik_{e+d}^-[P_{i,j}] + k^+[P_{i-1,j}][P_{1,0}] - k^+[P_{i,j}][P_{1,0}] + (ik_{e+d}^- + k_e^-)[P_{i+1,j}] \\ & -jk_{e+d}^-[P_{i,j}] + k^+[P_{i,j-1}][P_{0,1}] - k^+[P_{i,j}][P_{0,1}] + (jk_{e+d}^- + k_e^-)[P_{i,j+1}] \end{aligned} \tag{12}$$

where (i,j) are even. Similar equations can be written for the remaining three cases corresponding to (i odd, j odd), (i even, j odd), and (i odd, j even). The time dependence of monomer exchange was simulated using Eq. (12), keeping ΔG_e and ΔG_d fixed to the values obtained from fits of αB-crystallin size distributions, under the assumption that, at $t=0$, the only nonzero oligomer concentrations are those of $P_{i,0}$ and $P_{0,j}$. These values, in turn, can be obtained from distributions generated from MS data, as described above. The best fit of the experimental data to the time course predicted by Eq. (12) subject to the constraints of the size distribution equilibrium data gives $k^+[P_1]$, k_{e+d}^-, k_e^- that are reported in the text.

Acknowledgements

We thank Gillian Hilton, Nelson Barrera, Christine Slingsby and Sarah Meehan for stimulating discussions. This work was supported by grants from the Canadian Institutes of Health Research and the Natural Sciences and Engineering Research Council of Canada (L.E.K.). A.J.B. holds a Canadian

Institutes of Health Research postdoctoral fellowship, H.L. was a European Molecular Biology Organization fellow, C.V.R. is a Royal Society Professor, L.E.K. holds a Canadian Research Chair in Biochemistry, and J.L.P.B. is a Royal Society University Research Fellow.

Supplementary Data

Supplementary data associated with this article can be found, in the online version, at doi:10.1016/j.jmb.2011.07.016

References

1. Alberts, B. (1998). The cell as a collection of protein machines: preparing the next generation of molecular biologists. *Cell*, **92**, 291–294.
2. Robinson, C. V., Sali, A. & Baumeister, W. (2007). The molecular sociology of the cell. *Nature*, **450**, 973–982.
3. Levy, E. D., Boeri Erba, E., Robinson, C. V. & Teichmann, S. A. (2008). Assembly reflects evolution of protein complexes. *Nature*, **453**, 1262–1265.
4. Horwitz, J. (2009). Alpha crystallin: the quest for a homogeneous quaternary structure. *Exp. Eye Res.* **88**, 190–194.
5. Aquilina, J. A., Benesch, J. L. P., Bateman, O. A., Slingsby, C. & Robinson, C. V. (2003). Polydispersity of a mammalian chaperone: mass spectrometry reveals the population of oligomers in alphaB-crystallin. *Proc. Natl Acad. Sci. USA*, **100**, 10611–10616.
6. Haley, D. A., Horwitz, J. & Stewart, P. L. (1998). The small heat-shock protein, alphaB-crystallin, has a variable quaternary structure. *J. Mol. Biol.* **277**, 27–35.
7. Bagnéris, C., Bateman, O. A., Naylor, C. E., Cronin, N., Boelens, W. C., Keep, N. H. & Slingsby, C. (2009). Crystal structures of alpha-crystallin domain dimers of alphaB-crystallin and Hsp20. *J. Mol. Biol.* **392**, 1242–1252.
8. Clark, A. R., Naylor, C. E., Bagnéris, C., Keep, N. H. & Slingsby, C. (2011). Crystal structure of R120G disease mutant of human alphaB-crystallin domain dimer shows closure of a groove. *J. Mol. Biol.* **408**, 118–134.
9. Laganowsky, A., Benesch, J. L. P., Landau, M., Ding, L., Sawaya, M. R., Cascio, D. *et al.* (2010). Crystal structures of truncated alphaA and alphaB crystallins reveal structural mechanisms of polydispersity important for eye lens function. *Protein Sci.* **19**, 1031–1043.
10. Laganowsky, A. & Eisenberg, D. (2010). Non-3D domain swapped crystal structure of truncated zebrafish alphaA crystallin. *Protein Sci.* **19**, 1978–1984.
11. Jehle, S., Rajagopal, P., Bardiaux, B., Markovic, S., Kuhne, R., Stout, J. R. *et al.* (2010). Solid-state NMR and SAXS studies provide a structural basis for the activation of alphaB-crystallin oligomers. *Nat. Struct. Mol. Biol.* **17**, 1037–1042.
12. Haley, D. A., Horwitz, J. & Stewart, P. L. (1999). Image restrained modeling of alphaB-crystallin. *Exp. Eye Res.* **68**, 133–136.
13. Jehle, S., Vollmar, B. S., Bardiaux, B., Dove, K. K., Rajagopal, P., Gonen, T. *et al.* (2011). N-terminal domain of alphaB-crystallin provides a conformational switch for multimerization and structural heterogeneity. *Proc. Natl Acad. Sci. USA*, doi:10.1073/pnas.1014656108.
14. Peschek, J., Braun, N., Franzmann, T. M., Georgalis, Y., Haslbeck, M., Weinkauf, S. & Buchner, J. (2009). The eye lens chaperone alpha-crystallin forms defined globular assemblies. *Proc. Natl Acad. Sci. USA*, **106**, 13272–13277.
15. Horwitz, J. (2000). The function of alpha-crystallin in vision. *Semin. Cell Dev. Biol.* **11**, 53–60.
16. Tardieu, A. (1988). Eye lens proteins and transparency: from light transmission theory to solution X-ray structural analysis. *Annu. Rev. Biophys. Biophys. Chem.* **17**, 47–70.
17. van den Oetelaar, P. J., van Someren, P. F., Thomson, J. A., Siezen, R. J. & Hoenders, H. J. (1990). A dynamic quaternary structure of bovine alpha-crystallin as indicated from intermolecular exchange of subunits. *Biochemistry*, **29**, 3488–3493.
18. Bova, M. P., Ding, L. L., Horwitz, J. & Fung, B. K. (1997). Subunit exchange of alphaA-crystallin. *J. Biol. Chem.* **272**, 29511–29517.
19. Haslbeck, M., Franzmann, T., Weinfurtner, D. & Buchner, J. (2005). Some like it hot: the structure and function of small heat-shock proteins. *Nat. Struct. Mol. Biol.* **12**, 842–846.
20. McHaourab, H. S., Godar, J. A. & Stewart, P. L. (2009). Structure and mechanism of protein stability sensors: chaperone activity of small heat shock proteins. *Biochemistry*, **48**, 3828–3837.
21. Balch, W. E., Morimoto, R. I., Dillin, A. & Kelly, J. W. (2008). Adapting proteostasis for disease intervention. *Science*, **319**, 916–919.
22. Brady, J. P., Garland, D., Duglas-Tabor, Y., Robison, W. G., Jr, Groome, A. & Wawrousek, E. F. (1997). Targeted disruption of the mouse alpha A-crystallin gene induces cataract and cytoplasmic inclusion bodies containing the small heat shock protein alpha B-crystallin. *Proc. Natl Acad. Sci. USA*, **94**, 884–889.
23. Horwitz, J. (1992). Alpha-crystallin can function as a molecular chaperone. *Proc. Natl Acad. Sci. USA*, **89**, 10449–10453.
24. Dobson, C. M. (2003). Protein folding and misfolding. *Nature*, **426**, 884–890.
25. Ecroyd, H. & Carver, J. A. (2009). Crystallin proteins and amyloid fibrils. *Cell. Mol. Life Sci.* **66**, 62–81.
26. Benesch, J. L. P., Ruotolo, B. T., Simmons, D. A. & Robinson, C. V. (2007). Protein complexes in the gas phase: technology for structural genomics and proteomics. *Chem. Rev.* **107**, 3544–3567.
27. Heck, A. J. (2008). Native mass spectrometry: a bridge between interactomics and structural biology. *Nat. Methods*, **5**, 927–933.
28. Sharon, M. & Robinson, C. V. (2007). The role of mass spectrometry in structure elucidation of dynamic protein complexes. *Annu. Rev. Biochem.* **76**, 167–193.
29. Benesch, J. L. P. & Ruotolo, B. T. (2011). Mass spectrometry: an approach come of age for structural and dynamical biology. *Curr. Opin. Struct. Biol.* doi:10.1016/j.sbi.2011.08.002.

30. Aquilina, J. A., Benesch, J. L. P., Ding, L. L., Yaron, O., Horwitz, J. & Robinson, C. V. (2004). Phosphorylation of alphaB-crystallin alters chaperone function through loss of dimeric substructure. *J. Biol. Chem.* **279**, 28675–28680.
31. Aquilina, J. A., Benesch, J. L. P., Ding, L. L., Yaron, O., Horwitz, J. & Robinson, C. V. (2005). Subunit exchange of polydisperse proteins: mass spectrometry reveals consequences of alphaA-crystallin truncation. *J. Biol. Chem.* **280**, 14485–14491.
32. Benesch, J. L. P., Aquilina, J. A., Baldwin, A. J., Rekas, A., Stengel, F., Lindner, R. A., et al. The quaternary organization and dynamics of the molecular chaperone HSP26 are thermally regulated. Chem. Biol. 17, 1008–1017.
33. Painter, A. J., Jaya, N., Basha, E., Vierling, E., Robinson, C. V. & Benesch, J. L. P. (2008). Real-time monitoring of protein complexes reveals their quaternary organization and dynamics. *Chem. Biol.* **15**, 246–253.
34. Benesch, J. L. P., Ayoub, M., Robinson, C. V. & Aquilina, J. A. (2008). Small heat shock protein activity is regulated by variable oligomeric substructure. *J. Biol. Chem.* **283**, 28513–28517.
35. Benesch, J. L. P., Aquilina, J. A., Ruotolo, B. T., Sobott, F. & Robinson, C. V. (2006). Tandem mass spectrometry reveals the quaternary organization of macromolecular assemblies. *Chem. Biol.* **13**, 597–605.
36. Benesch, J. L. P. (2009). Collisional activation of protein complexes: picking up the pieces. *J. Am. Soc. Mass Spectrom.* **20**, 341–348.
37. Michiel, M., Skouri-Panet, F., Duprat, E., Simon, S., Ferard, C., Tardieu, A. & Finet, S. (2009). Abnormal assemblies and subunit exchange of alphaB-crystallin R120 mutants could be associated with destabilization of the dimeric substructure. *Biochemistry*, **48**, 442–453.
38. Baldwin, A. J., Hilton, G. R., Lioe, H., Bagneris, C., Benesch, J. L. P. & Kay, L. E. (2011). Quaternary dynamics of aB-crystallin as a direct conseqeunce of localised tertiary fluctuations in the C-terminus. *J. Mol. Biol.* Under review. doi:10.1016/j.jmb.2011.07.017.
39. Hall, D. & Minton, A. P. (2002). Effects of inert volume-excluding macromolecules on protein fiber formation. I. Equilibrium models. *Biophys. Chem.* **98**, 93–104.
40. Baldwin, A. J., Knowles, T. P. J., Tartaglia, G., Fitzpatrick, A., Devlin, G., Shammas, S. *et al.* (2011). Metastability of native proteins and the phenomenon of amyloid formation. *J. Am. Chem. Soc.* In press. doi: 10.1021/ja2017703.
41. Oosawa, F. & Kasai, M. (1962). A theory of linear and helical aggregations of macromolecules. *J. Mol. Biol.* **4**, 10–21.
42. van Holde, K. E., Johnson, W. C. & Ho, P. S (2006). In *Principles of Physical Biochemistry*, (2nd ed). Prentice Hall, NJ.
43. Jehle, S., van Rossum, B., Stout, J. R., Noguchi, S. M., Falber, K., Rehbein, K. *et al.* (2009). alphaB-crystallin: a hybrid solid-state/solution-state NMR investigation reveals structural aspects of the heterogeneous oligomer. *J. Mol. Biol.* **385**, 1481–1497.
44. Oosawa, F. & Asakura, S. (1975). *Thermodynamics of the Polymerisation of Protein.* Academic, New York, NY.
45. Alsallaq, R. & Zhou, H. X. (2008). Electrostatic rate enhancement and transient complex of protein–protein association. *Proteins: Struct., Funct., Bioinf.* **71**, 320–335.
46. Clark, A. R., Naylor, C. E., Bagnéris, C., Keep, N. H. & Slingsby, C. (2011). Crystal structure of R120G disease mutant of human alphaB-crystallin domain dimer shows closure of a groove. *J. Mol. Biol.* **408**, 118–134.
47. Douglas, J. F., Dudowicz, J. & Freed, K. F. (2009). Crowding induced self-assembly and enthalpy-entropy compensation. *Phys. Rev. Lett.* **103**, 135701.
48. Tsai, C. J., del Sol, A. & Nussinov, R. (2008). Allostery: absence of a change in shape does not imply that allostery is not at play. *J. Mol. Biol.* **378**, 1–11.
49. Villar, G., Wilber, A. W., Williamson, A. J., Thiara, P., Doye, J. P., Louis, A. A. *et al.* (2009). Self-assembly and evolution of homomeric protein complexes. *Phys. Rev. Lett.* **102**, 118106.
50. Kim, K. K., Kim, R. & Kim, S. H. (1998). Crystal structure of a small heat-shock protein. *Nature*, **394**, 595–599.
51. van Montfort, R. L., Basha, E., Friedrich, K. L., Slingsby, C. & Vierling, E. (2001). Crystal structure and assembly of a eukaryotic small heat shock protein. *Nat. Struct. Biol.* **8**, 1025–1030.
52. Haley, D. A., Bova, M. P., Huang, Q. L., McHaourab, H. S. & Stewart, P. L. (2000). Small heat-shock protein structures reveal a continuum from symmetric to variable assemblies. *J. Mol. Biol.* **298**, 261–272.
53. Stengel, F., Baldwin, A. J., Painter, A. J., Jaya, N., Basha, E., Kay, L. E. *et al.* (2010). Quaternary dynamics and plasticity underlie small heat shock protein chaperone function. *Proc. Natl Acad. Sci. USA*, **107**, 2007–2012.
54. Van Montfort, R., Slingsby, C. & Vierling, E. (2001). Structure and function of the small heat shock protein/alpha-crystallin family of molecular chaperones. *Adv. Protein Chem.* **59**, 105–156.
55. Farahbakhsh, Z. T., Huang, Q. L., Ding, L. L., Altenbach, C., Steinhoff, H. J., Horwitz, J. & Hubbell, W. L. (1995). Interaction of alpha-crystallin with spin-labeled peptides. *Biochemistry*, **34**, 509–516.
56. Augusteyn, R. C. (2004). Dissociation is not required for alpha-crystallin's chaperone function. *Exp. Eye Res.* **79**, 781–784.
57. Bennardini, F., Wrzosek, A. & Chiesi, M. (1992). Alpha B-crystallin in cardiac tissue. Association with actin and desmin filaments. *Circ. Res.* **71**, 288–294.
58. Koretz, J. F., Doss, E. W. & LaButti, J. N. (1998). Environmental factors influencing the chaperone-like activity of alpha-crystallin. *Int. J. Biol. Macromol.* **22**, 283–294.
59. Poon, S., Rybchyn, M. S., Easterbrook-Smith, S. B., Carver, J. A., Pankhurst, G. J. & Wilson, M. R. (2002). Mildly acidic pH activates the extracellular molecular chaperone clusterin. *J. Biol. Chem.* **277**, 39532–39540.
60. Bassnett, S. & Duncan, G. (1986). Variation of pH with depth in the rat lensmeasured by double-barrelled ion-sensitive microelectrodes. In *The Lens: Transparency and Cataract Topics in Ageing Research in Europe* (Duncan, G., ed.), Vol. 6, pp. 77–85. Eurage, Rijswijk, The Netherlands.
61. Mathias, R. T., Riquelme, G. & Rae, J. L. (1991). Cell to cell communication and pH in the frog lens. *J. Gen. Physiol.* **98**, 1085–1103.

62. Poole-Wilson, P. A. (1978). Measurement of myocardial intracellular pH in pathological states. *J. Mol. Cell. Cardiol.* **10**, 511–526.
63. Ecroyd, H., Meehan, S., Horwitz, J., Aquilina, J. A., Benesch, J. L. P., Robinson, C. V. *et al.* (2007). Mimicking phosphorylation of alphaB-crystallin affects its chaperone activity. *Biochem. J.* **401**, 129–141.
64. Meehan, S., Knowles, T. P., Baldwin, A. J., Smith, J. F., Squires, A. M., Clements, P. *et al.* (2007). Characterisation of amyloid fibril formation by small heat-shock chaperone proteins human alphaA-, alphaB- and R120G alphaB-crystallins. *J. Mol. Biol.* **372**, 470–484.
65. Hernandez, H. & Robinson, C. V. (2007). Determining the stoichiometry and interactions of macromolecular assemblies from mass spectrometry. *Nat. Protoc.* **2**, 715–726.
66. Sobott, F., Hernandez, H., McCammon, M. G., Tito, M. A. & Robinson, C. V. (2002). A tandem mass spectrometer for improved transmission and analysis of large macromolecular assemblies. *Anal. Chem.* **74**, 1402–1407.
67. Fraser, G. W. (2002). The ion detection efficiency of microchannel plates (MCPs). *Int. J. Mass Spectrom.* **215**, 13–30.
68. Bova, M. P., McHaourab, H. S., Han, Y. & Fung, B. K. (2000). Subunit exchange of small heat shock proteins. Analysis of oligomer formation of alphaA-crystallin and Hsp27 by fluorescence resonance energy transfer and site-directed truncations. *J. Biol. Chem.* **275**, 1035–1042.